Published in final edited form as:
JALA Charlottesv Va. 2010 December 31; 15(6): 426–432. doi:10.1016/j.jala.2010.05.004.

Electrothermal Fluid Manipulation of High-Conductivity Samples for Laboratory Automation Applications

Mandy L. Y. Sin[†], **Vincent Gau**[⊥], **Joseph C. Liao**[+], and **Pak Kin Wong**[†,|,*]

[†] Department of Aerospace and Mechanical Engineering, University of Arizona, PO Box 210119, Tucson, AZ 85721 USA

[⊥] GeneFluidics Inc, 2540 Corporate Place, Suite B-101, Monterey Park, CA 91754 USA

[+] Department of Urology, Stanford University, 300 Pasteur Drive, S-287, Stanford, CA 94305-5118 USA

[|] Biomedical Engineering and Bio5 Institute, University of Arizona, Tucson, Arizona 85721, USA

Abstract

Electrothermal flow is a promising technique in microfluidic manipulation toward laboratory automation applications, such as clinical diagnostics and high throughput drug screening. Despite the potential of electrothermal flow in biomedical applications, relative little is known about electrothermal manipulation of highly conductive samples, such as physiological fluids and buffer solutions. In this study, the characteristics and challenges of electrothermal manipulation of fluid samples with different conductivities were investigated systematically. Electrothermal flow was shown to create fluid motion for samples with a wide range of conductivity when the driving frequency was above 100 kHz. For samples with low conductivities (below 1 S/m), the characteristics of the electrothermal fluid motions were in quantitative agreement with the theory. For samples with high conductivities (above 1 S/m), the fluid motion appeared to deviate from the model as a result of potential electrochemical reactions and other electrothermal effects. These effects should be taken into consideration for electrothermal manipulation of biological samples with high conductivities. This study will provide insights in designing microfluidic devices for electrokinetic manipulation of biological samples toward laboratory automation applications in the future.

Introduction

The development of automated microfluidic systems poses great promises for a variety of medical diagnostic applications[1-3]. While extensive research efforts have been devoted to integrate various transduction mechanisms, including optical, inertial, interfacial, and electrochemical sensing, the transducers often require sample preparation components for handling clinical samples[4-7]. The implementation of the sample preparation modules, which critically determines the overall performance of the system, can often be cumbersome, labor intensive and time-consuming and represents a major challenge for laboratory automation[8, 9]. Among numerous microfluidic techniques, AC electrokinetics is one of the most promising approaches for addressing this fundamental hurdle in laboratory automation[10-12].

[*] To whom correspondence should be addressed. Tel.: +1-520-626-2215; fax: +1-520-621-8191; pak@email.arizona.edu.

AC electrokinetics is especially effective in the micro and nano domains and can be easily integrated with other microfluidic components. Furthermore, combinations of different electrokinetics phenomena allow fundamental fluidic operations including concentration, separation, mixing, and pumping to be performed in the same platform[13-15]. Electrokinetics has also been applied in various mechanobiological applications[16, 17]. All these features render electrokinetics one of the most promising approaches for developing fully integrated microfluidic diagnostic systems for laboratory automation[18, 19].

Most electrokinetic techniques, such as dielectrophoresis and AC electroosmosis, are effective only in low conductivity fluids. Electrothermal flow, on the other hand, is effective in fluids that have a wide range of conductivity. The effectiveness of electrothermal flow in samples with high conductivities, such as biological buffers and physiological fluids (on the order of 1 S/m), contributes to its general applicability in laboratory automation applications. Electrothermal flow is typically observed at frequencies above 100 kHz[20]. When an external electrical field is applied across the electrode, Joule heating creates temperature gradients near the electrode. The temperature gradient induces permittivity and conductivity gradients. The interaction between the electric field and the gradients, as a result, creates a bulk electrical force causing fluid motion.

A theoretical model has been developed previously to reveal the characteristics of electrothermal flow[21, 22]. Neglecting convection that is relatively slow compared to thermal diffusion in typical operating conditions, the temperature distribution at equilibrium can be estimated by balancing Joule heating and thermal diffusion.

$$k\nabla^2 T+\sigma E^2=0 \tag{1}$$

where k is the thermal diffusivity, T is the temperature of the medium, σ is the conductivity of the medium, and E is the applied electric field. Rearranging equation 1 provides an order of magnitude estimation of the temperature rise,

$$\Delta T \approx \sigma V^2/k \tag{2}$$

Equation 2 describes the general dependence of the temperature rise and more accurate temperature estimation has also be performed[21, 22]. Since conductivity and permittivity gradients are induced due to the temperature gradient, an electrical force on the bulk fluid is created as a result of the interaction between the electric field and the gradients. The time average electrothermal force, $\langle f_E \rangle$, has been estimated to be

$$\langle f_E \rangle = -\frac{1}{2}\left[\left(\frac{\nabla\sigma}{\sigma}-\frac{\nabla\varepsilon}{\varepsilon}\right)\cdot\overline{E}_0\frac{\varepsilon\overline{E}_0}{1+(\omega\tau)^2}+\frac{1}{2}|E_0|^2\nabla\varepsilon\right] \tag{3}$$

where ω is the angular frequency of the applied potential, ε is the permittivity, and E_0 is the magnitude of the electric field. The first and second terms on the right hand side of equation 3 represent the Coulomb force and the dielectric force, respectively. The charge relaxation time, τ, is the ratio between the permittivity and the conductivity, $\tau = \varepsilon/\sigma$. An analytical expression of the time average electrothermal force has been derived for a parallel electrode with a small gap.

$$\langle f_E \rangle = -M(\omega, T)\left(\frac{\varepsilon\sigma V_{rms}^4}{2k\pi^3 r^3 T}\right)\left(1 - \frac{2\theta}{\pi}\right)\hat{n}_\theta \tag{4}$$

$$M(\omega, T) = \left(\frac{T/\sigma\,\partial\sigma/\partial T - T/\varepsilon\,\partial\varepsilon/\partial T}{1+\omega^2\tau^2} + \frac{1}{2}\frac{T}{\varepsilon}\frac{\partial\varepsilon}{\partial T}\right) \tag{5}$$

where r and θ are the radial and angular coordinates. $M(\omega,T)$ represents the frequency dependence of the electrothermal force. The induced electrothermal profile can be estimated by considering the Stokes equations.

$$\eta\nabla^2\overline{v} - \nabla p + \overline{f} = 0 \tag{6}$$

$$\nabla \cdot v = 0 \tag{7}$$

where η is the viscosity, v is the velocity, p is the pressure, and f is the bulk fluid force. To the first order approximation, the electrothermal velocity can be approximated by $\overline{v} \approx \left|\overline{f}\right| \frac{l^2}{\eta}$ and is roughly proportional to the bulk fluid force.

This theoretical analysis reveals several key characteristics and practical considerations of electrothermal fluid manipulation. Firstly, the temperature rise approximation indicates that the temperature of the sample can be over 100 °C in some conditions. This is especially important when the conductivity of the sample is high. A high temperature could lead to degradation of the samples (e.g., proteins) and other unwanted electrothermal effects. Secondly, electrothermal flow depends on the applied frequency. The Coulomb force dominates at low frequency while the dielectric force dominates at a high frequency. The crossover of the dominance and change in the flow direction occur at a frequency on the order of the inverse of the charge relaxation time. Third, the electrothermal force and the fluid velocity have strong voltage dependences (to the fourth power) on the applied voltage. Within a laboratory automation context, it is the most effective operating parameter for regulating the electrothermal for sample preparation applications.

Recent studies of electrothermal flow have demonstrated that a biotin-streptavidin binding assay can be enhanced by electrothermal stirring[23, 24]. Micropumps based on electrothermal flow have also been proposed by using an array of asymmetric pairs of electrodes[25, 26]. On the other hand, a combination of electrothermal flow and other electrokinetic effects have been demonstrated for particle trapping, concentration, separation, mixing, and pumping[27-30]. In addition to Joule heating induced electrothermal flow, opto-electrical fluid motion has been reported for particle manipulation[31-33]. Nevertheless, relatively little is known about the fundamental characteristics and practical limits for electrothermal manipulation of fluids with high conductivities. In this paper, we perform a systematic investigation on electrothermal manipulation of fluids with a wide range of conductivities. The results could potentially serve as guidelines in the design of electrothermal flow based microfluidic devices for laboratory automation applications.

Materials and Methods

A concentric electrode design was applied to generate three dimensional vortices in a microfluidic chamber. The outer diameter and gap distance of the concentric electrodes are 550 μm and 50 μm (Figure 1a). The electrodes were deposited by evaporating 300 nm gold on a glass substrate with a 50 nm chromium adhesion layer and were patterned by lift-off. The microfluidic chamber was created by placing a cover slip and spacers of 170 μm on top of the substrate. The AC driving voltage was generated by a function generator (HP, 33120A). The inner and outer electrodes were connected to the driving signal and the ground, respectively. The potential drop across the microelectrode was monitored by a digital storage oscilloscope (GW Instek, GDS-1102) and reported as the voltage values.

The experiments were performed using buffer of 1× Tris-EDTA with conductivities from 0.01 - 22 S/m. The conductivity of the solution was adjusted by addition of sodium chloride. The solutions were seeded with 200 nm florescent particles (Invitrogen, F8810) for flow visualization. All velocity measurements were performed 100 μm above the gap of the concentric electrode to avoid the dielectrophoretic effect on the tracer particles[34]. The microfluidic chamber was loaded onto an epi-fluorescence microscope (Leica, DMI 4000B). The particle motion was captured with a digital CCD camera (Image Source, DMK31AF03) at 30 frames per second. All experiments were performed at room temperature (22 °C).

Fluorescence images were analyzed with Matlab and ImageJ. At least 8 particles were traced for each velocity measurement and the results were reported as the mean ± standard error of the mean. The exponent, e, of the voltage dependence of the electrothermal velocity, v, was fitted using the power law relationship, $v = CV^e$, where V is the root mean square voltage (V_{rms}) and C is an empirical constant depending on the geometry of the electrode and other operating conditions. The results were reported as the mean ± standard error of the fit.

Results

In the experiment, three dimensional fluid motions were observed on the concentric electrode. The flow patterns were similar for different operating conditions. Figure 1b show a representative image of the flow pattern by tracing the particle trajectory. The conductivity was 1 S/m, and the applied voltage and frequency were 6 V peak-to-peak and 200 kHz, respectively. It should be noted that the fluid motion extended to regions as much as 300 μm outside the electrode, which is approximately the same as the radius of the outer electrode.

The fluid velocity was measured at different frequencies (100 kHz - 13 MHz) to investigate the frequency dependence of the observed fluid motion. Lower voltages were applied to samples with higher conductivities to avoid electrolysis and bubble formation. Figure 2 shows the frequency dependence of the fluid motion. For 0.01 S/m, the velocity at low frequency was approximately constant. The flow motion changed to the opposite direction at high frequency and the frequency of the transition occurred approximately at 5 MHz. For 0.1 S/m, a decreasing trend of the fluid velocity was observed at high frequency (from 10-15 MHz). Higher frequency was not characterized due to the limitation of the operating frequency range of the function generator. For higher conductivities (1.3 and 22 S/m), the electrothermal velocities remained constant in the frequency range tested.

The frequency dependence of electrothermal flow estimated by the model is shown in Figure 3. The model suggested that the electrothermal force and crossover frequency increased with the conductivity of the medium. Since the electrothermal force is linearly proportional to the velocity, we normalized the force estimated by the model and the velocity measured from the experiment to compare the frequency dependence of the fluid motion (Figure 4). For 0.01 and 0.1 S/m, excellent agreement was obtained between the experiment and the model.

For 0.01 S/m, the predicted crossover frequency was 4.46 MHz and the value observed was 5 MHz. For 1 S/m and 22 S/m, the crossover frequencies were predicted to be 0.446 GHz and 9.8 GHz, which were outside the frequency range tested. As expected, the electrothermal effects remained constant in both the experiment and the model for the frequency range being examined. Furthermore, we normalized the force estimated by the model and the experimentally measured fluid velocity with the fourth power of the applied voltage (see equation 3) at 200 kHz to study the conductivity dependence (Figure 5). For low conductivities (0.01 to 1 S/m), the normalized velocity scaled linearly with the conductivity as suggested by the model. Both the frequency and conductivity dependence studies indicated that the observed fluid motion was a result of electrothermal flow. For high conductivity (22 S/m), while the fluid motion displayed similar frequency dependences, the amplitude of the velocity deviated significantly from the value predicted.

In order to better understand the effect of the conductivity, the voltage dependence of the fluid velocity were characterized. The applied frequency was 500 kHz. Figure 6 shows the voltage dependence of the fluid velocity from 0.01 S/m to 22 S/m. Generally, the velocity increased with the applied voltage and the conductivity. The velocity-voltage relationship displaced the power-law dependence. According to the model, the electrothermal force should have a fourth power dependence on the electric field. Figure 7 summarizes and compares the scaling exponents predicted in the model and observed in the experiment. For conductivities between 0.01 S/m to 1 S/m, the velocity approximately scaled to the fourth power to the applied voltage. It should be noted that AC electroosmosis and dielectrophoresis have second power dependence on the applied voltage. These further supported that the observed fluid motion was a result of electrothermal flow and the model was able to capture the frequency dependence of the observed fluid motion at low conductivity. However, the exponents deviated from the model and decreased from 3.8 to below 1 when the conductivity increased from 1 to 22 S/m. The decreasing trend of the exponent at high conductivity (> 5 S/m) was likely to be the results of other phenomena that are sensitivity to the conductivity of the sample.

Discussions

Our results suggest electrothermal flow is a dominant electrohydrodynamic effect when the applied frequency is above 100 kHz. The observed fluid motion cannot be explained by other electrohydrodynamic effects, which have different frequency and voltage dependences. For instance, AC electroosmosis is only effective at low frequency (below 100 kHz) and has a second power dependence on the applied voltage[10]. On the other hand, Joule heating induced temperature gradient can create a difference in fluid density and results in buoyancy force[21, 22]. The buoyancy force, f_B, is given by,

$$f_B = \frac{\partial \rho_m}{\partial T} \Delta T g \tag{8}$$

where ρ_m is the fluid density, g is the standard gravity and ΔT is the temperature rise, which can be estimated from equation (2). Numerical calculation reveals that the ratio between the buoyancy force and the Coulomb force is less than 0.1 in our experimental condition. This suggests that the buoyancy force is unlikely to be a dominant effect in our experiment conditions.

Our experimental data suggest that the electrothermal flow is applicable to samples with a wide range of conductivity. As shown in Figure 5, similar electrothermal velocity can be obtained in samples with conductivities spanning across 3 orders of magnitude by adjusting

the applied voltage. A lower voltage is needed for manipulating a sample with a higher conductivity. This presents a unique advantage of electrothermal flow for biomedical applications. The technique is highly effective with physiological fluids including blood urine and saliva, which have conductivities on the order of 1 S/m.

In the experiment, we observed discrepancy between the experimental data and the model. The aberrancy could be a result of the idealistic assumptions in the model. With a highly conductive buffer, electrochemical reaction at the electrode surfaces, which is not considered in the model, may no longer be neglected. In fact, we observed degradation of the electrode surfaces (Fig. 8). These electrochemical reactions may reduce the effective potential across the electrode and the resulting electrothermal effect. Secondly, the temperature rise is assumed to be small in the derivation of the electrothermal force. Nevertheless, the estimated temperature rise can reach above 100°C based on the order of magnitude estimation. This presents uncertainties in the linear approximation and the boundary conditions applied in the model. As a result, the assumption that the buoyancy effect is negligible may no longer be valid. Furthermore, evaporation, which could further increase the effective conductivity of the sample, became significant in our experiment. We noticed that by applying AC potential with a peak-to-peak voltage of 6 V and 200 kHz, the conductivity of the buffer has increased from 10 S/m to 13 S/m in 5 minutes. Further theoretical and experimental investigation, e.g., measuring the temperature distribution of fluids with different conductivities, will be necessary to elucidate the roles of these electrothermal, buoyancy and electrochemical effects on electrothermal fluid manipulation.

Conclusions

Electrothermal flow is one of the most effective AC electrokinetic techniques for laboratory automation due to its effectiveness at physiological conductivity (~ 1 S/m). Despite the discrepancy in the model, our results demonstrated that electrothermal flow is highly effective from the manipulation of fluids with a wide range of conductivities. Our result will serve as a guideline for performing effective sample preparation procedures using the electrothermal processing. In situ characterization of the sample conductivity using impedance spectroscopy or other techniques could be integrated into the microfluidic system for handling samples with unknown conductivities.

Acknowledgments

This work is supported by NIH NIAID (1U01AI082457), NSF (CBET-0930900), and NSF (ECCS-0900899).

References

1. Rane TD, et al. Counting single molecules in sub-nanolitre droplets. Lab on a Chip 2010;10:161–164. [PubMed: 20066242]
2. Chen CH, et al. Antimicrobial susceptibility testing using high surface-to-volume ratio microchannels. Anal Chem 2010;82:1012–1019. [PubMed: 20055494]
3. Yang H, Luk VN, Abeigawad M, Barbulovic-Nad I, Wheeer AR. A World-to-Chip Interface for Digital Microfluidics. Analytical Chemistry 2009;81:1061–1067. [PubMed: 19115860]
4. Kim J, et al. Applications, Techniques, and Microfluidic Interfacing for Nanoscale Biosensing. Microfluidics and Nanofluidics 2009;7:149–167.
5. Mach KE, et al. Multiplex pathogen identification for polymicrobial urinary tract infections using biosensor technology: a prospective clinical study. The Journal of urology 2009;182:2735–2741. [PubMed: 19837423]
6. Choi S, Yang YM, Chae J. Surface plasmon resonance protein sensor using Vroman effect. Biosensors & Bioelectronics 2008;24:893–899.

7. Zhang CY, Yeh HC, Kuroki MT, Wang TH. Single-quantum-dot-based DNA nanosensor. Nature Materials 2005;4:826–831.
8. Chiu ML, et al. Matrix Effect - A Challenge Toward Automation of Molecular Analysis. Journal of the Association for Laboratory Automation. 2010 in press.
9. Sviridov D, Hortin GL. Urine albumin measurement: effects of urine matrix constituents. Clin Chim Acta 2009;404:140–143. [PubMed: 19332047]
10. Wong PK, Wang TH, Deval JH, Ho CM. Electrokinetics in micro devices for biotechnology applications. IEEE-ASME Transactions on Mechatronics 2004;9:366–376.
11. Hughes MP. AC electrokinetics: applications for nanotechnology. Nanotechnology 2000;11:124–132.
12. Oh J, Hart R, Capurro J, Noh H. Comprehensive analysis of particle motion under non-uniform AC electric fields in a microchannel. Lab on a Chip 2009;9:62–78. [PubMed: 19209337]
13. Wong PK, Chen CY, Wang TH, Ho CM. Electrokinetic bioprocessor for concentrating cells and molecules. Analytical Chemistry 2004;76:6908–6914. [PubMed: 15571340]
14. Sin MLY, Shimabukuro Y, Wong PK. Hybrid electrokinetics for separation, mixing, and concentration of colloidal particles. Nanotechnology 2009;20:165701. [PubMed: 19420574]
15. Sin MLY, Gau V, Liao JC, Haake DA, Wong PK. Active Manipulation of Quantum Dots using AC Electrokinetics. J Phys Chem C 2009;113:6561–6565.
16. Wong PK, Tan W, Ho CM. Cell relaxation after electrodeformation: effect of latrunculin A on cytoskeletal actin. Journal of Biomechanics 2005;38:529–535. [PubMed: 15652551]
17. Kim DH, Wong PK, Park J, Levchenko A, Sun Y. Microengineered platforms for cell mechanobiology. Annual Review of Biomedical Engineering 2009;11:203–233.
18. Wang TH, Wong PK. Transforming Microfluidics into Laboratory Automation. Journal of the Association for Laboratory Automation. 2010 in press.
19. Lawi W, et al. A Microfluidic Cartridge System for Multiplexed Clinical Analysis. Journal of the Association for Laboratory Automation 2009;14:407–412. [PubMed: 20161584]
20. Green NG, Ramos A, Gonzalez A, Castellanos A, Morgan H. Electrothermally induced fluid flow on microelectrodes. Journal of Electrostatics 2001;53:71–87.
21. Ramos A, Morgan H, Green NG, Castellanos A. Ac electrokinetics: a review of forces in microelectrode structures. Journal of Physics D-Applied Physics 1998;31:2338–2353.
22. Castellanos A, Ramos A, Gonzalez A, Green NG, Morgan H. Electrohydrodynamics and dielectrophoresis in microsystems: scaling laws. Journal of Physics D-Applied Physics 2003;36:2584–2597.
23. Feldman HC, Sigurdson M, Meinhart CD. AC electrothermal enhancement of heterogeneous assays in microfluidics. Lab on a Chip 2007;7:1553–1559. [PubMed: 17960285]
24. Sigurdson M, Wang DZ, Meinhart CD. Electrothermal stirring for heterogeneous immunoassays. Lab on a Chip 2005;5:1366–1373. [PubMed: 16286967]
25. Wu J, Lian M, Yang K. Micropumping of biofluids by alternating current electrothermal effects. Applied Physics Letters 2007;90
26. Lian M, Islam N, Wu J. AC electrothermal manipulation of conductive fluids and particles for lab-chip applications. Iet Nanobiotechnol 2007;1:36–43. [PubMed: 17506595]
27. Park S, Koklu M, Beskok A. Particle Trapping in High-Conductivity Media with Electrothermally Enhanced Negative Dielectrophoresis. Analytical Chemistry 2009;81:2303–2310. [PubMed: 19215119]
28. Ng WY, Goh S, Lam YC, Yang C, Rodriguez I. DC-biased AC-electroosmotic and AC-electrothermal flow mixing in microchannels. Lab on a Chip 2009;9:802–809. [PubMed: 19255662]
29. Gagnon ZR, Chang HC. Electrothermalac electro-osmosis. Applied Physics Letters 2009;94
30. Lin Y, Shiomi J, Maruyama S, Amberg G. Electrothermal flow in dielectrophoresis of single-walled carbon nanotubes. Physical Review B 2007;76
31. Green NG, Ramos A, Gonzalez A, Castellanos A, Morgan H. Electric field induced fluid flow on microelectrodes: the effect of illumination. Journal of Physics D-Applied Physics 2000;33:L13–L17.

32. Gonzalez A, Ramos A, Morgan H, Green NG, Castellanos A. Electrothermal flows generated by alternating and rotating electric fields in microsystems. Journal of Fluid Mechanics 2006;564:415–433.

33. Kumar A, Williams SJ, Wereley ST. Experiments on opto-electrically generated microfluidic vortices. Microfluidics and Nanofluidics 2009;6:637–646.

34. Meinhart C, Wang DZ, Turner K. Measurement of AC electrokinetic flows. Biomedical Microdevices 2003;5:139–145.

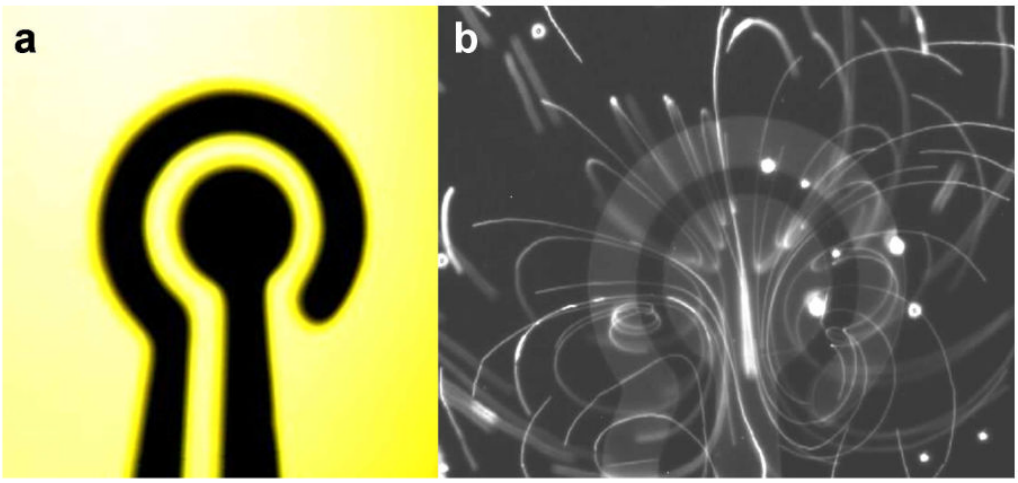

Fig. 1.
(a) Schematic of the concentric electrode for characterizing electrothermal flow. (b) Visualization of the particle trajectories by overexposure the CCD camera for 13 sec.

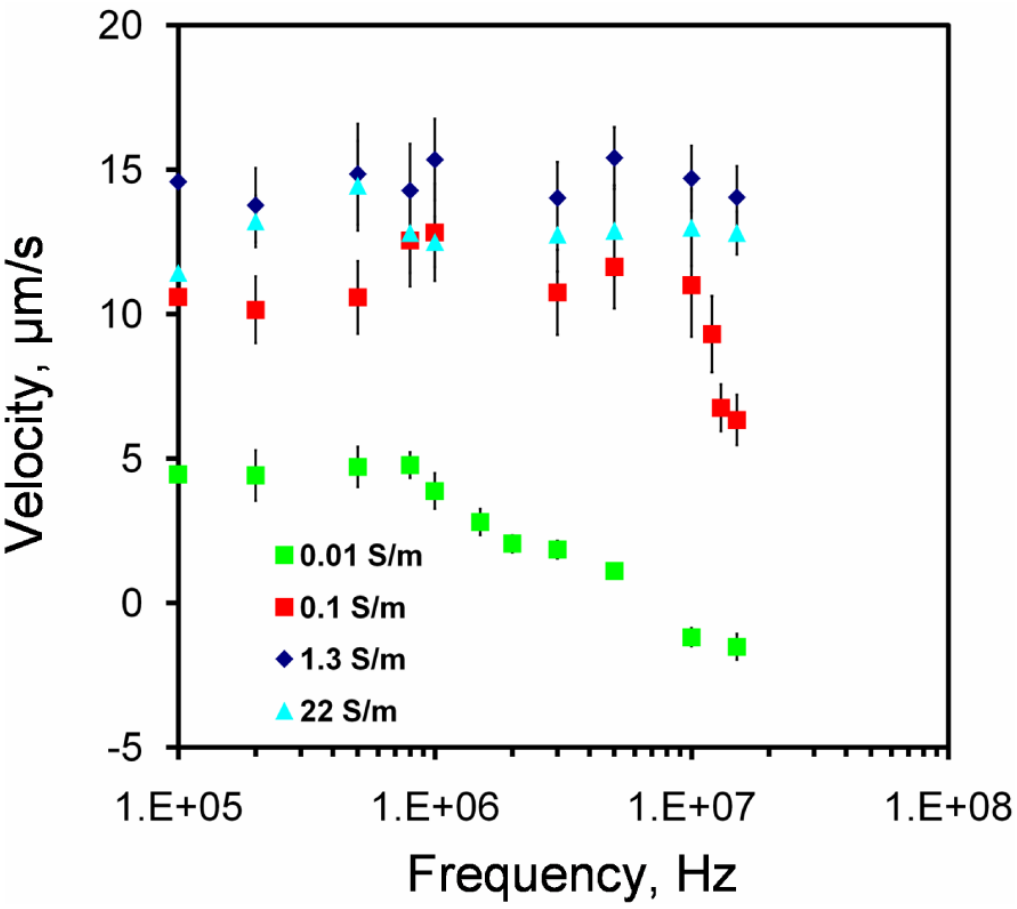

Fig. 2.

Frequency dependence of the fluid velocity. Applied voltages are sinusoidal waveforms with peak-to-peak voltage of 20 V, 16 V, 10 V and 8 V for conductivities of 0.01 Sm^{-1}, 0.1 Sm^{-1}, 1.3 Sm^{-1}, and 22 Sm^{-1}, respectively. Error bars represent the standard error of the mean.

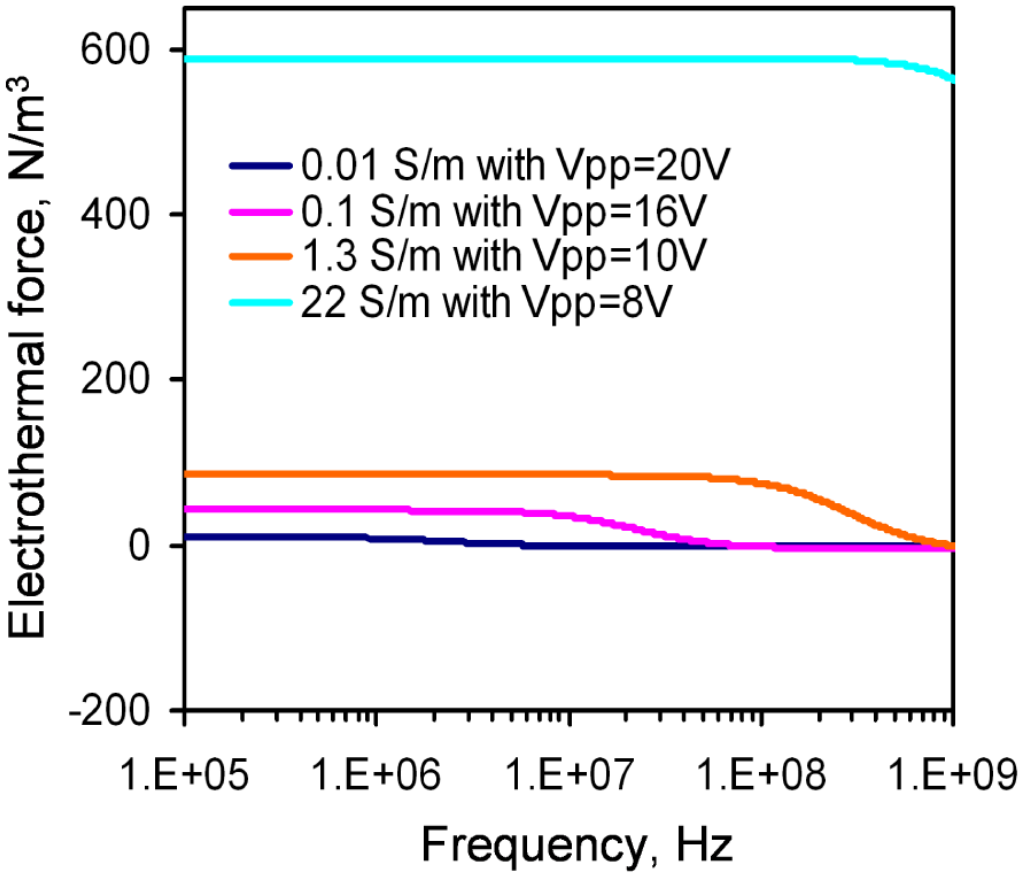

Fig. 3.

The frequency dependence of the electrothermal force for different conductivities calculated by the model. Voltages are sinusoidal waveforms with peak-to-peak voltage of 20 V, 16 V, 10 V, and 8 V for conductivities of 0.01 Sm^{-1}, 0.1 Sm^{-1}, 1.3 Sm^{-1}, and 22 Sm^{-1}, respectively.

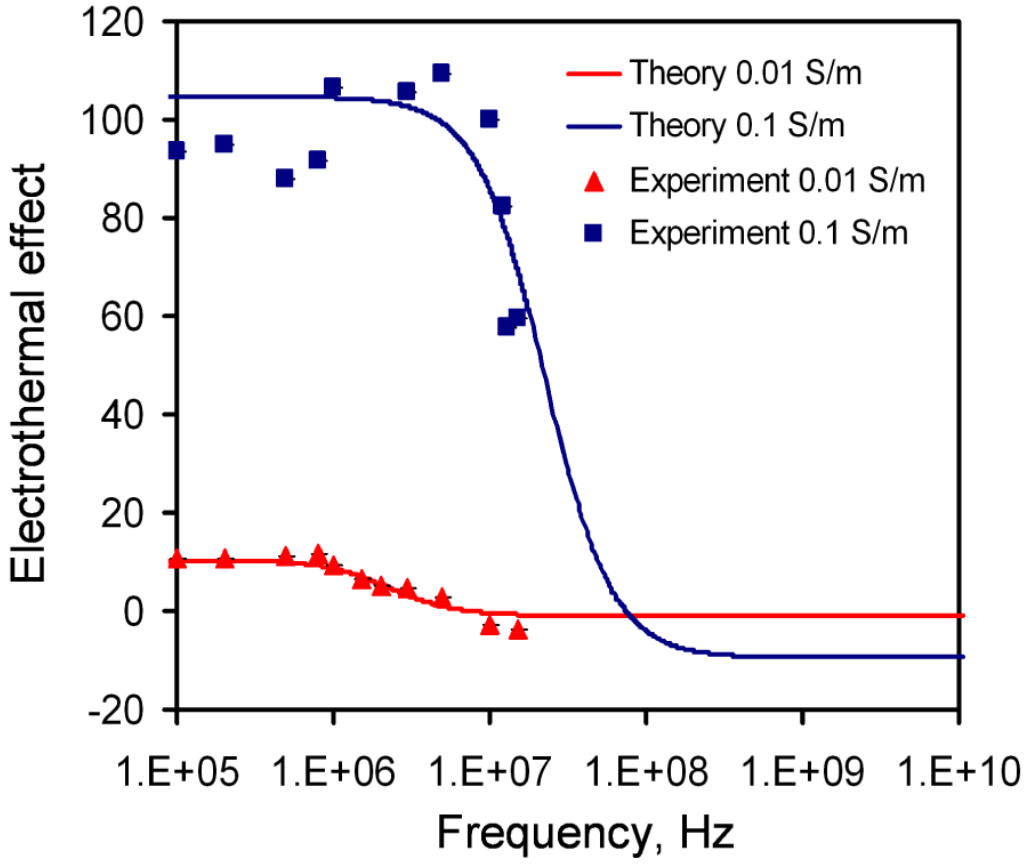

Fig. 4.
Comparison of the frequency dependence of the experimental results with the model for samples with conductivities of 0.01 Sm^{-1} and 0.1 Sm^{-1}.

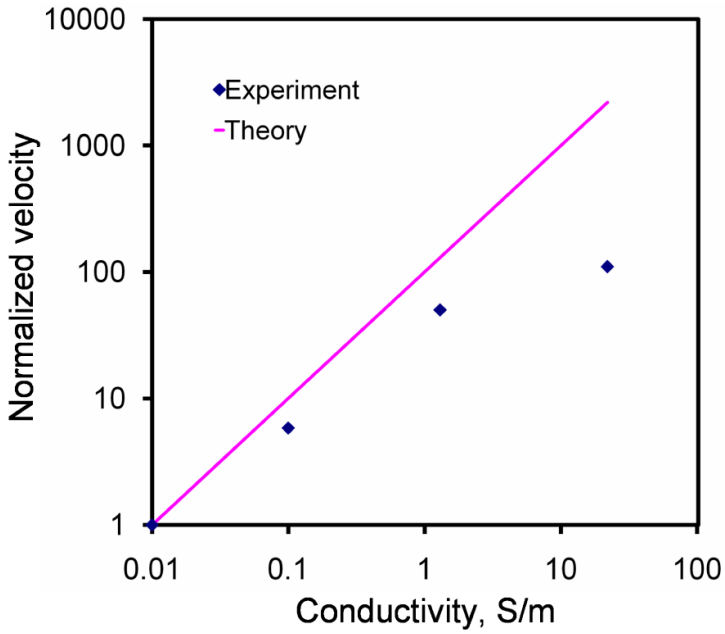

Fig. 5.

Comparison of the conductivity dependence of the experimental results with the theoretical calculation. The velocities were normalized with the fourth power the applied root-mean-square voltage to compare the conductivity dependence. Error bars represent the standard error of the mean.

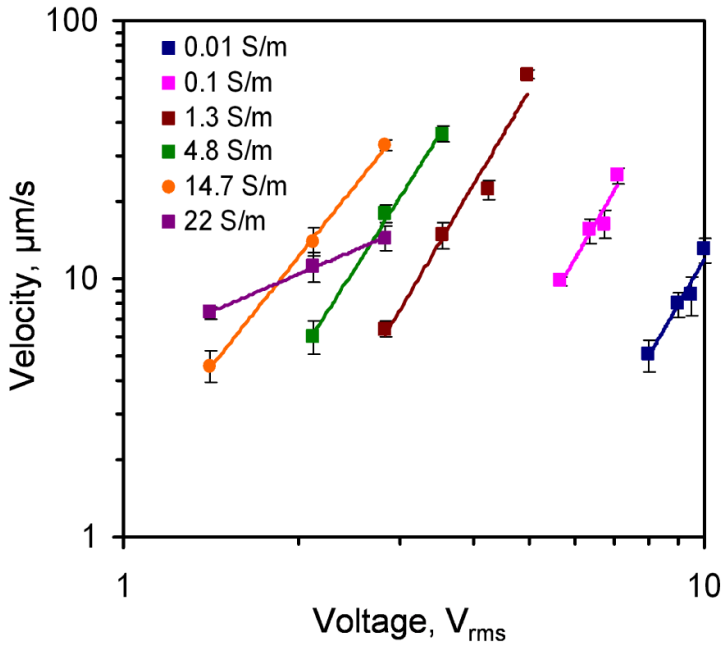

Fig. 6.
Voltage dependence of the fluid velocity at 200 kHz. Data represent mean ± standard error of the mean.

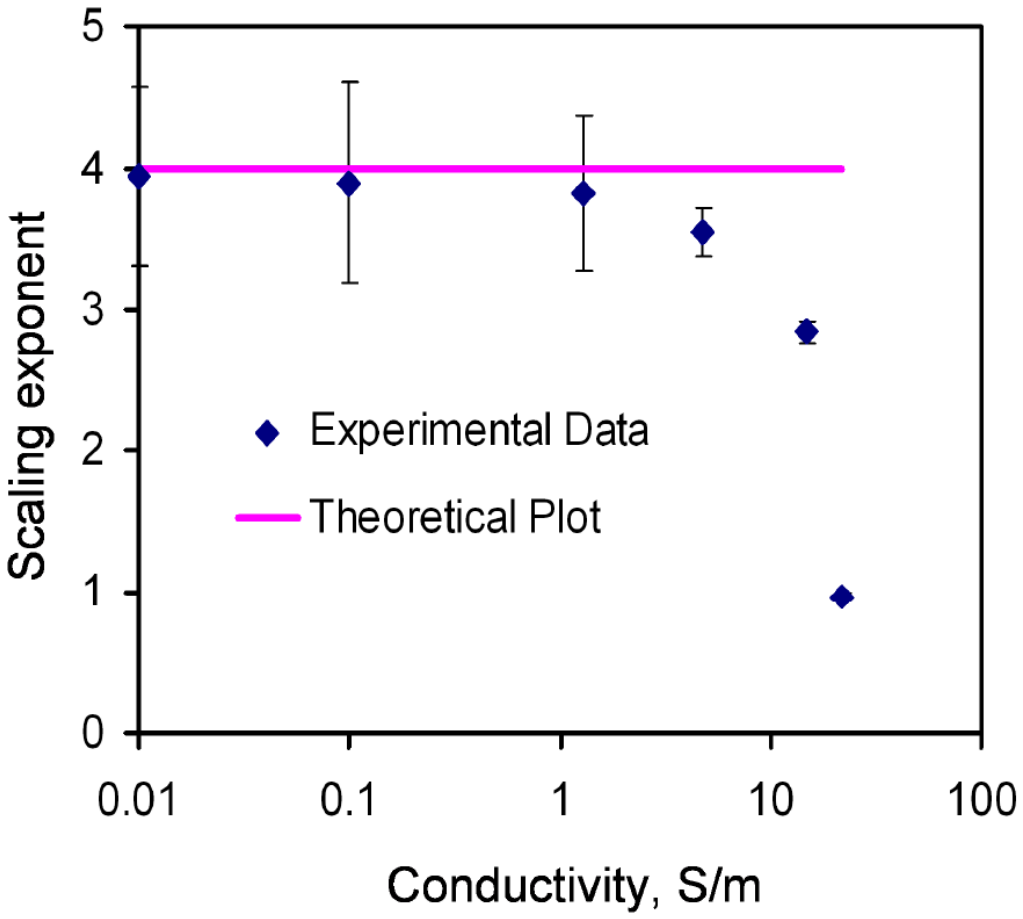

Fig. 7.
Comparison of the power exponent for the electrothermal force and the applied electric field of the experimental data with the theory at different conductivities. Error bars represent the standard error of the fit.

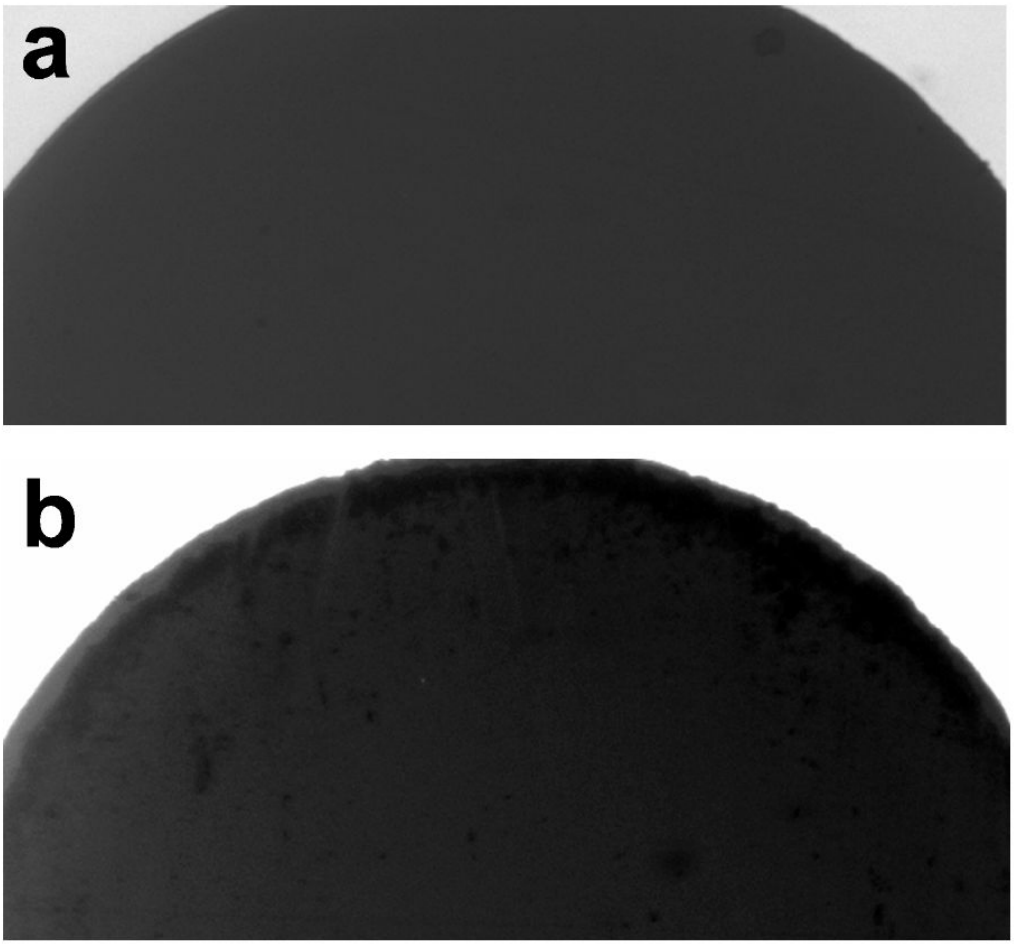

Fig. 8.
The electrode surface (a) before and (b) after the application of a voltage of 8 V peak to peak and frequency of 200 kHz for 1 min. The conductivity of the sample was 5 S/m.